Setting the scene for Gaia and LAMOST
Proceedings IAU Symposium No. 298, 2013
S. Feltzing, G. Zhao, N. A. Walton & P. A. Whitelock, eds.

doi:10.1017/S1743921313006339

Chemodynamical Simulations of the Milky Way Galaxy - Inhomogeneous Chemical Enrichment

Chiaki Kobayashi

Centre for Astrophysics Research, School of Physics, Astronomy and Mathematics, University of Hertfordshire; College Lane, Hatfield AL10 9AB, UK
email: c.kobayashi@herts.ac.uk

Abstract. The predictions of our chemodynamical simulations from cosmological initial conditions are as follows: The disk formed Inside-out. Metallicity radial and vertical gradients exist, but no [α/Fe] radial gradient. Metallicity radial gradient is steeper at higher redshifts. The [α/Fe]-[Fe/H] relation is caused by the delayed enrichment of Type Ia supernovae (not with long lifetimes, but with the metallicity effect). The bulge formed through the assembly of small gas-rich galaxies at high redshifts. [α/Fe] is higher, [Mn/Fe] is lower, [(Na, Al)/Fe] are higher than the disk. Metallicity and [α/Fe] vertical gradients exist, which is caused by the increase of metal-rich and low [α/Fe] populations at lower latitudes. Bars may form later, which may show boxy and cylindrical rotation. Half of thick disk stars (kinetically selected) come from minor mergers. [α/Fe] is higher, and [Mn/Fe] is lower than the thin disk, but [(Na, Al, Cu, Zn)/Fe] are lower than the bulge. There are metallicity vertical, weak metallicity radial, and no [α/Fe] radial gradients. It would be interesting to compare the predictions with other models such as radial mixing, disk heating, and clumpy disks.

For the solar neighborhood, the frequency distributions of elements from oxygen to zinc are in excellent agreement not only for the average values but also for the scatter. In chemodynamical simulations, chemical enrichment takes place inhomogeneously, and the scatter originates from a combination of various effects - mergers, migration, and in-situ. The inhomogeneous enrichment is important in reproducing observed nitrogen abundances, and also in understanding elemental abundance patterns of dwarf spheroidal galaxies and carbon-enhanced damped Lyman α systems.

Keywords. Galaxy: abundances — Galaxy: evolution — Galaxy: formation — methods: numerical — stars: supernovae

1. Introduction

Different elements and isotopes are produced from stars on different timescales. Therefore, elemental and isotopic abundance ratios evolve as a function of time in a galaxy. The observed elemental and isotopic abundance ratios are the fossils that retain the formation and evolutionary history of the galaxy. This approach is often called *galactic archaeology*. Nucleosynthesis yields have recently been updated and a complete yield table is provided for $1-300M_{\odot}$ (Nomoto, Kobayashi & Tominaga 2013, hereafter NKT13). Galactic chemical evolution models (Kobayashi *et al.* 2006; Kobayashi *et al.* 2011a) are in excellent agreement with observations except for some elements. The ν-process plays an essential role in the production of F (Kobayashi *et al.* 2011c), while multi-dimensional calculation is necessary for Ti (Maeda & Nomoto 2003).

Galactic chemical evolution has been studied with so-called *one-zone models* (also called monolithic models in the cosmological context) for many years. In one-zone models, it is assumed that the interstellar medium (ISM) of the region under consideration is well

mixed instantaneously and has a uniform chemical composition. In reality, the ISM is not well mixed and more-realistic models have been proposed. *Stochastic models* (e.g., Argast *et al.* 2002) can involve inhomogeneous mixing statistically. *Hierarchical (semi-analytic) models* (Tumlinson 2006) include cosmological mass accretion.

Thanks to the development of high-performance computers and numerical techniques, it became possible to calculate chemical enrichment combined with 3D hydrodynamical simulations, which are called *chemodynamical simulations* (e.g., Kobayashi & Nakasato 2011, hereafter KN11, and references therein). With such chemodynamical simulations, positions, kinematics, ages, metallicities, and elemental abundances of star particles are obtained. Thus, the scatter of observational data and the effect of inhomogeneous mixing may be studied. These are the predictions that can be, and should be, compared with future observations with high-resolution multi-object spectrographs such as APOGEE, HERMES, and Gaia-ESO surveys.

2. Chemodynamical Simulations

We use a hydrodynamical code that includes relevant physical processes such as radiative cooling, star formation, supernova feedback, and chemical enrichment from core-collapse supernovae (SNe II and HNe), Type Ia supernovae (SNe Ia), and asymptotic giant branch (AGB) stars. The progenitor model of SNe Ia is based on the single degenerate scenario, and taking account of the metallicity effects of white dwarf winds (Kobayashi *et al.* 1998), the lifetime distribution functions are calculated as in Kobayashi & Nomoto (2009). See Kobayashi (2004), Kobayashi, Springel & White (2007), and KN11 for the details. We use ΛCDM initial conditions, so that any galaxy forms through the successive merging of subgalaxies with various masses. The initial condition is chosen in order to avoid major mergers at $z \lesssim 2$, which is necessary to retain the disk structure. In this simulated galaxy, the bulge is formed by the initial starburst that is induced by the assembly of gas-rich sub-galaxies with stellar masses of $\sim 5 - 10 \times 10^9 M_\odot$ and gas fractions of $0.2 - 0.4$ at $z \gtrsim 3$. Because of the angular momentum, the gas accretes onto the plane forming a rotationally supported disk that grows from inside out. In the disk, star formation takes place with a longer timescale, which is maintained not by the slow gas accretion, but by the self-regulation due to supernova feedback. Many satellite galaxies successively come in and disrupt, and half of thick disk stars have formed in merging galaxies.

In a real galaxy, the star formation history is not so simple and in particular the interstellar medium (ISM) is not homogeneous at any time, which is different from one-zone chemical evolution models. The effects of inhomogeneous enrichment can be summarized as follows. (I) There is a local variation in star formation and metal flow by the inflow and outflow of the ISM. (II) Heavy elements are distributed via stellar winds and supernovae, and the elemental abundance ratios depend on the metallicity and mass of progenitor stars. (III) The ISM may be mixed before the next star formation by other effects such as diffusion and turbulence. (IV) There is a mixing of stars due to dynamical effects such as merging and migration.

In chemodynamical simulation (KN11), hydrodynamics and chemical enrichment are solved self-consistently throughout the galaxy formation. Star formation and chemical enrichment depend on the local density. With our feedback scheme, star particles obtain heavy elements from the gas particles from which the stars form. Gas particles obtain heavy elements only when they pass within a feedback radius of dying star particles. The mass and metallicity dependencies are included by looking at the age and metallicity of progenitor star particles. Nucleosynthesis yields also depend on the explosion energy,

https://doi.org/10.1017/S1743921313006339 Published online by Cambridge University Press

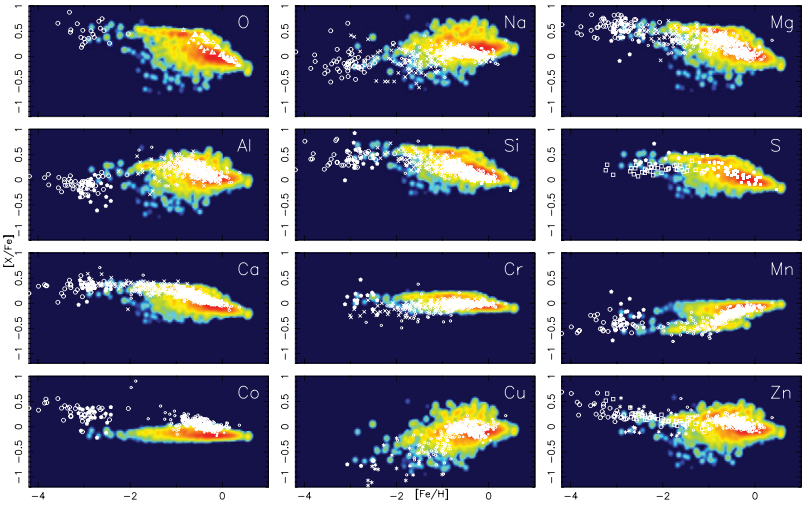

Figure 1. [X/Fe]-[Fe/H] relations in the solar neighborhood at $z = 0$. The contours show the frequency distribution of stars in the simulated galaxies, where red is for the highest frequency. See KN11 for the observational data sources (white dots).

which has not been included. Because it is not possible to resolve supernova ejecta, the size of feedback region, or the number of gas particle that receive feedback, is given by a parameter. This will account for some of gas-phase mixing. Therefore, (I), (II), (IV) are naturally included but (III) is probably not enough.

2.1. *Elemental abundances in the solar neighborhood*

Figure 1 shows the frequency distribution of elemental abundances of stars in the solar neighborhood at present. The dots are for the observations of individual stars, which are in excellent agreement with our simulation (contours) not only for the averaged values, but also for the scatter. See KN11 for the observational data sources and 3D/NLTE corrections. Note that the large number of metal-poor stars in these observational data is due to the selection bias. In the observed metallicity distribution functions, the metallicity is peaked at [Fe/H] ~ 0.

- α elements — O, Mg, Si, S, and Ca show the same relation; At the beginning, only SNe II contribute, and [α/Fe] shows a plateau ([α/Fe]~ 0.5). Around [Fe/H] ~ -1, SNe Ia start to occur, which produce more iron than α elements. This delayed enrichment of SNe Ia causes the decrease in [α/Fe] with increasing [Fe/H]. Around [Fe/H] ~ -1, the scatter looks a bit larger than observed. This may be because the mixing of heavy elements among gas particles is not included in our model. From the comparison of the [α/Fe] scatter between simulations and observations, it is possible to put constraints on the unsolved physics of supernova explosion and mixing of the ISM.
- Odd-Z elements — Na, Al, and Cu show a decreasing trend toward lower metallicity since the nucleosynthesis yields of these elements strongly depend on the metallicity of progenitor stars. Na and Al also show a decreasing trend toward higher metallicity due to SNe Ia, which is shallower than that of α elements. [Na/Fe] at [Fe/H] $\gtrsim -1$ may be slightly larger than observed. The large scatter is caused by the metallicity dependence of yields. In our chemodynamical simulations, there is only a week correlation between the metallicities of supernova progenitors and those of the surrounding ISM. If the ejected metals are diluted, the ISM metallicity and the metallicity of stars that form from the

https://doi.org/10.1017/S1743921313006339 Published online by Cambridge University Press

ISM become lower than the progenitor metallicity. The scatter starts increasing at [Fe/H] ~ -2 in this simulation, which looks consistent with the observations.

• Iron-peak elements — The scatter of Cr and Co is very small since there is not very much variety in the SN II yields and [(Cr, Co)/Fe] is almost ~ 0 for SNe Ia. For Cr, since a dependence on the temperature of the observed stars has been reported, we plot the Cr II abundance for low metallicity, which is consistent with our simulation. For Co, an increasing trend toward lower metallicity is seen in the observations, which is not realized in the simulation. This is due to the input of supernova yields, and cannot be solved with different star formation histories or initial conditions. This could be solved if we adopt higher energy and/or higher fraction of HNe where more Co and Zn are synthesized.

• Zinc — Zn is one of the most important elements for supernova physics. [Zn/Fe] is about ~ 0 for a wide range of metallicities, which can only be generated by such large contribution of HNe. In detail, there is a small oscillating trend; [Zn/Fe] is 0 at [Fe/H] ~ 0, increases to be 0.2 at [Fe/H] ~ -0.5, decreases to be 0 at [Fe/H] ~ -2, then increases toward lower metallicity. This is characteristic in our SN Ia model, and is consistent with the observations. Theoretically, Zn production depends on many parameters; ^{64}Zn is synthesized in the deepest region of HNe, while neutron-rich isotopes of zinc $^{66-70}$Zn are produced by neutron-capture processes, which are larger for higher metallicity massive SNe II. The scatter at $-1.5 \lesssim$ [Fe/H] $\lesssim -0.5$ is larger than observed, which is caused by the dependence of the Zn yield on the metallicity and mass. The increasing trend toward lower metallicity in the observations could be generated with the same effects as for Co.

• Manganese — Mn is a characteristic element and is more produced by SNe Ia relative to iron. From [Fe/H] ~ -1, [Mn/Fe] shows an increasing trend toward higher metallicity, which is caused by the delayed enrichment of SNe Ia. Mn is also an odd-Z element, and the Mn yield depends on the metallicity both for SNe II and SNe Ia. At [Fe/H] $\lesssim -2$, the scatter in the simulation is a bit smaller than observed. Since SNe Ia do not contribute at such low metallicity, the [Mn/Fe] scatter, if it is real, should stem from the SN II yields depending on the remnant mass and the electron fraction Y_e that is related to the mechanism of supernova explosion. In the supernova ejecta, Mn and Cr are synthesized in the relatively outer regions compared to Cr, Zn and the majority of Fe. Therefore, relatively high [(Mn, Cr)/Fe] and low [(Co, Zn)/Fe] are obtained with faint SNe with relatively large remnant masses (black holes; Kobayashi *et al.* 2011b).

2.2. *Dependence on locations*

Although the same star formation criteria are applied for all particles in the simulation, the resultant star formation histories are different for different components. The initial starburst is induced by the assembly, and most of stars in the bulge and halo are formed at this stage. In the disk, the SFR is regulated mainly by supernova feedback (see Fig. 6 of KN11 for the SFRs). This difference is clearly seen in the age-metallicity relations (see Fig. 8 of KN11). In the solar neighborhood, the average metallicity reaches [Fe/H] ~ 0 at $t \sim 2$ Gyr and does not show strong evolution for $t \gtrsim 2$ Gyr. This is consistent with observations (e.g., Casagrande *et al.* 2011). In the bulge, star formation takes place more quickly, and thus the chemical enrichment timescale is much shorter than in the disk. The age-metallicity relation shows a more rapid increase than in the disk. The maximum metallicity reaches super-solar values ([Fe/H] ~ 1) at $t \sim 2$ Gyr. Although the SFR becomes small after ~ 5 Gyr, a few stars form at $\gtrsim 5$ Gyr. These have super-solar metallicity in general and the average metallicity does not show time evolution.

The difference in the chemical enrichment timescales results in a difference in the elemental abundance ratios (see Fig.10 of KN11). In the bulge, the chemical enrichment timescale is so short that the metallicity reaches super-solar values before SNe Ia

https://doi.org/10.1017/S1743921313006339 Published online by Cambridge University Press

contribute. Thus, the [α/Fe] plateau continues to [Fe/H] $\sim +0.3$. In this simulated galaxy, some new stars are still forming in the bulge, which in general have super-solar metallicity and low [α/Fe] because of the large contribution from SNe Ia. The two distinct populations are seen in the [α/Fe]-[Fe/H] relations. See KN11 for the [X/Fe]-[Fe/H] diagrams of the bulge and the thick disk.

Figure 2 shows the distribution functions of [X/Fe] in the solar neighborhood (solid line), bulge (dashed line), and thick disk (dotted line). α elements show the double peak distributions, and the [α/Fe]-rich peak is at the same [α/Fe] for the solar neighborhood, bulge, and thick disk. On the other hand, Na, Al, Cu, and Zn show the single peak distributions in the solar neighborhood, but the double peak distributions in the bulge. On the average, Na, Al, Cu, and Zn are much more enhanced in the bulge, and (Na, Al, Cu, Zn)/α is larger than in the solar neighborhood. In the thick disk, the [(Na, Al, Cu, Zn)/Fe] distributions are rather similar to the solar neighborhood because the metallicity is not as high as in the bulge. The stellar population of the thick disk is neither thin-disk like nor bulge like. For the thick disk stars, the star formation timescale is as short as in the bulge, but the chemical enrichment efficiency is not as high as in the bulge. This is because half of the thick disk stars have already formed in satellite galaxies before they accrete onto the disk, and the metals have been ejected from the satellite galaxies by the galactic winds.

The left panel of Figure 3 shows the radial and vertical metallicity gradients of stars at present. The radial gradient of stars becomes flatter at higher distances from the plane, which seems to be consistent with the SDSS observations (Cheng *et al.* 2012). At $|z| = 0-0.5$ kpc (solid line), the stellar radial gradient is $\Delta[\mathrm{M/H}]_*/\Delta r = -0.025$ dex/kpc. This is flatter than the radial gradient of the ISM (dotted line), which is $\Delta[\mathrm{M/H}]_{\mathrm{g}}/\Delta r = -0.049$ dex/kpc at $|z| = 0 - 0.5$ kpc.

The time evolution of these gradients are important for determining the major physical process the disk formation (Pilkington *et al.* 2012). In chemodynamical simulations like our model, metallicity radial gradients are steeper at higher redshifts (see KN11 for the figure). This time evolution is consistent with the observations of lensed disk galaxies at $z = 2$ (Jones *et al.* 2010) and $z = 1.49$ (Yuan *et al.* 2011). On the other hand,

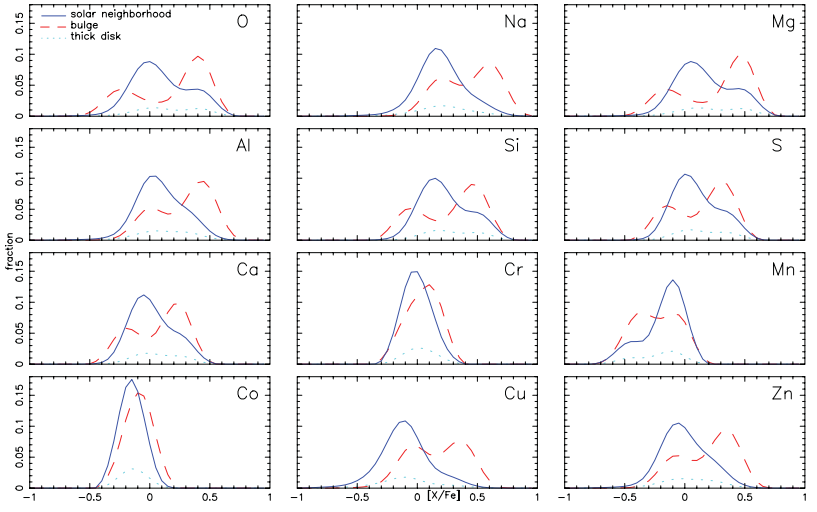

Figure 2. Distribution functions of the elemental abundance ratios relative to iron [X/Fe] in the solar neighborhood (solid line), bulge (dashed line), and thick disk (dot-dashed line) at $z = 0$.

https://doi.org/10.1017/S1743921313006339 Published online by Cambridge University Press

classic monolithic collapse models often predict opposite evolution, and migration may have much faster evolution (Schönrich & Binney 2009). Note that an inverse gradient is shown at $z \sim 3$ (Cresci *et al.* 2010), but there is no stable disk at such a high redshift in chemodynamical simulations from cosmological initial conditions, and this observation is not suitable for the discussion of Milky Way-size disks.

However, there are no gradients in [O/Fe] in disks, being consistent with the RAVE observations (Ruchti *et al.* 2011). The right panel of Figure 3 shows the radial and vertical [O/Fe] gradients of stars at present. There are metallicity gradients but not [O/Fe] gradients. These two results suggest that the chemical enrichment efficiency is higher in the center but the star formation timescale does not so much depend on the radius.

In the bulge, there is a vertical gradient in [O/Fe]. In order to break down this result, Figure 4 shows metallicity (left panel) and [O/Fe] (right panel) distribution functions at various latitudes. At $|z| < 1$ kpc, the metallicity distribution span a wide range of metallicity (see KN11 for the comparison with observational data). At high latitudes, the metal-rich population decreases, and the mean metallicity becomes low. At $|z| < 2$ kpc, there is a significant number of stars enriched by SNe Ia, which have [O/Fe] lower than 0.2. The duration of star formation is longer at lower latitudes, because supernova feedback is not enough to blow bulge winds in this simulation. There is a possibility that the feedback from the central super-massive black hole may cause a bulge wind.

2.3. *Local inhomogeneous effect*

In this section, we discuss three processes that cause a scatter of stellar abundances. The first two processes are in the effect (IV), and the third process consists of the effects (I)-(III). Figure 5 shows how each process affects on stellar populations in the solar neighborhood, by selecting stars from the locations when the stars formed.

(1) Accretion of stars in merging satellites that have a different evolutionary history. Usually chemical enrichment efficiency is low because of the small potential well. No age-metallicity relation is expected. In Figure 5, there is no stars at [Fe/H] $\gtrsim 0$, and no time evolution. There is not very much contribution from SNe Ia. The most metal-poor population is originated from this process as in the halo stars.

(2) Migration of stars along the disk plane. Stars formed in the center can be located in the solar neighborhood at present. Because of the metallicity gradients, metallicity

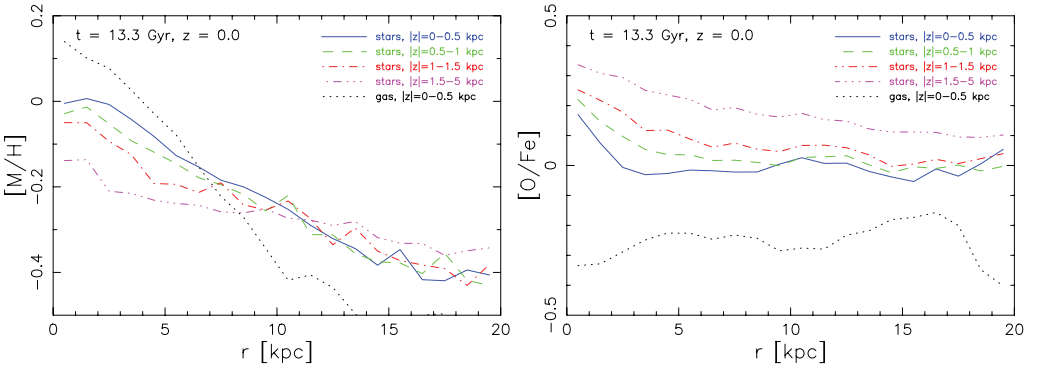

Figure 3. Radial gradients of metallicity (left panel) and [O/Fe] (right panel) for stars at the height $|z| = 0 - 0.5$ (solid line), $0.5 - 1$ (dashed line), $1 - 1.5$ (dot-dashed line), and $1.5 - 5$ (triple-dot-dashed line) kpc. The dotted lines show the radial gradients of gas at $|z| = 0 - 0.5$ kpc. The abundances are mass-weighted.

https://doi.org/10.1017/S1743921313006339 Published online by Cambridge University Press

can be high. No age-metallicity relation is expected. In Figure 5, [Fe/H] is as high as ~ 0, and no time evolution. Most of these stars are disk stars and enriched by SNe Ia.

(3) There is an intrinsic scatter in the stars formed in the solar neighborhood because star formation and chemical enrichment depend on local densities (in situ). In Figure 5, there is no old stars at $t \lesssim 2$ Gyr because the disk grow inside-out. The age-metallicity relation is seen from (t, [Fe/H])=(6 Gyr, -0.5) to (13 Gyr, $+0.5$). The [O/Fe]-[Fe/H] relation is seen from [Fe/H] ~ -1 to $+0.5$. These is no metal-poor stars with [Fe/H] ~ -1.4, which suggest that there is pre-enrichment from pre-existing supernovae. However, there is still a significant scatter in both relations. This is the *local* inhomogeneous enrichment effect.

Different from one-zone chemical evolution models, the following phenomena occur in the case of inhomogeneous enrichment: (i) The age-metallicity relation is weak. In other words, the most metal-poor stars are not always the oldest stars. In our simulations, the metallicity of the first enriched stars reaches [Fe/H] ~ -3. At later times, the star forming region becomes denser, and both metal richer and poorer stars than [Fe/H] ~ -3 appear. (ii) SNe Ia can affect the elemental abundance ratios at [Fe/H] $\lesssim -1$ even with the metallicity inhibition of SNe Ia. The SN Ia contribution is characterised by low [α/Fe] and high [Mn/Fe]. (iii) The scatter of elemental abundance ratios becomes large if the supernova yield depends on progenitor metallicity such as Na. (iv) Some of CEMP/NEMP stars can be explained with the local enrichment from AGB stars even without the binary effect. In fact, the observed [N/O]-[O/H] trend can be reproduced with our simulation without including the effect of rotating massive stars.

Figure 6 shows the [N/O]-[O/H] relations. Here we use a different simulation of a galaxy with a better initial condition and higher resolution. The basic properties are show in Scannapieco *et al.* (2012). Even at low metallicities, there are a significant number of stars with [N/O] $\gtrsim 0$, which are locally enriched by AGB stars. This means that additional sources of primary nitrogen such as rotating massive stars are not required if the inhomogeneous enrichment is taken into account.

3. Dwarf Spheroidal Galaxies

The *local* inhomogeneous effect is in particular important in small systems with low star formation rates, i.e., in dwarf spheroidal galaxies (dSphs). The [α/Fe] ratios of

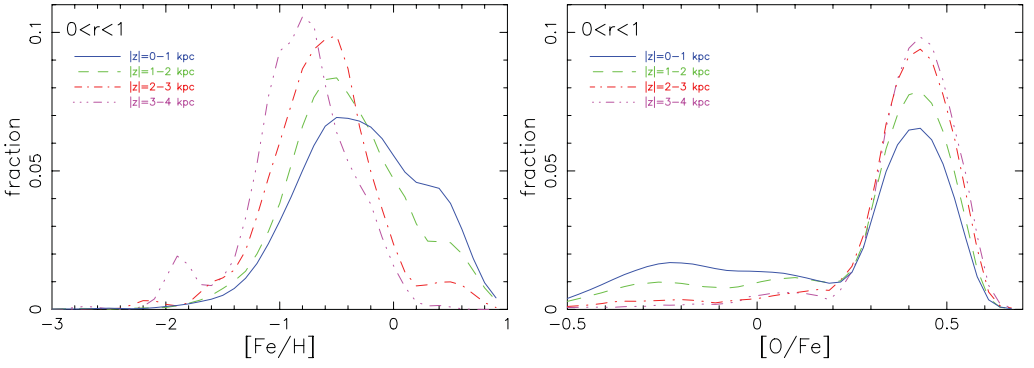

Figure 4. Vertical gradients of metallicity (left panel) and [O/Fe] (right panel) in the bulge. The lines show metallicity and [O/Fe] distribution functions of stars at the height $|z| = 0 - 1$ (solid line), $1 - 2$ (dashed line), $2 - 3$ (dot-dashed line), and $3 - 4$ (triple-dot-dashed line) kpc and at the radius $0 \leqslant r \leqslant 1$.

https://doi.org/10.1017/S1743921313006339 Published online by Cambridge University Press

stars in dSphs such as Fornax and Sagittarius are lower than those of the Galactic halo stars (Tolstoy *et al.* 2009). This difference is often interpreted to indicate a larger contribution of SNe Ia in dSphs than that of the solar neighborhood. However, the observed [Mn/Fe] ratios of dSph stars are as low as those of the Galactic halo stars (McWilliam, Rich & Smecker-Hane 2003; Romano, Cescutti & Matteucci 2011), which rejects SN Ia contribution in dSphs. These abundance patterns are more consistent with the yields of low-mass core-collapse supernovae ($\lesssim 20M_{\odot}$). The ejected masses of α particles highly depend on the progenitor mass, while the ejected iron mass does not vary very much for normal SNe II (Figs 1-4 in Kobayashi *et al.* 2006). Indeed, the contribution of low-mass supernovae can be dominant in very low star formation rates. As a result, the initial mass function is truncated at $\sim 20M_{\odot}$. This effect has not been included in chemodynamical simulations.

Also in the solar neighborhood, there are some low [α/Fe] stars, which have kinematics distinct from those of high [α/Fe] stars and may be debris of accreted satellite. These

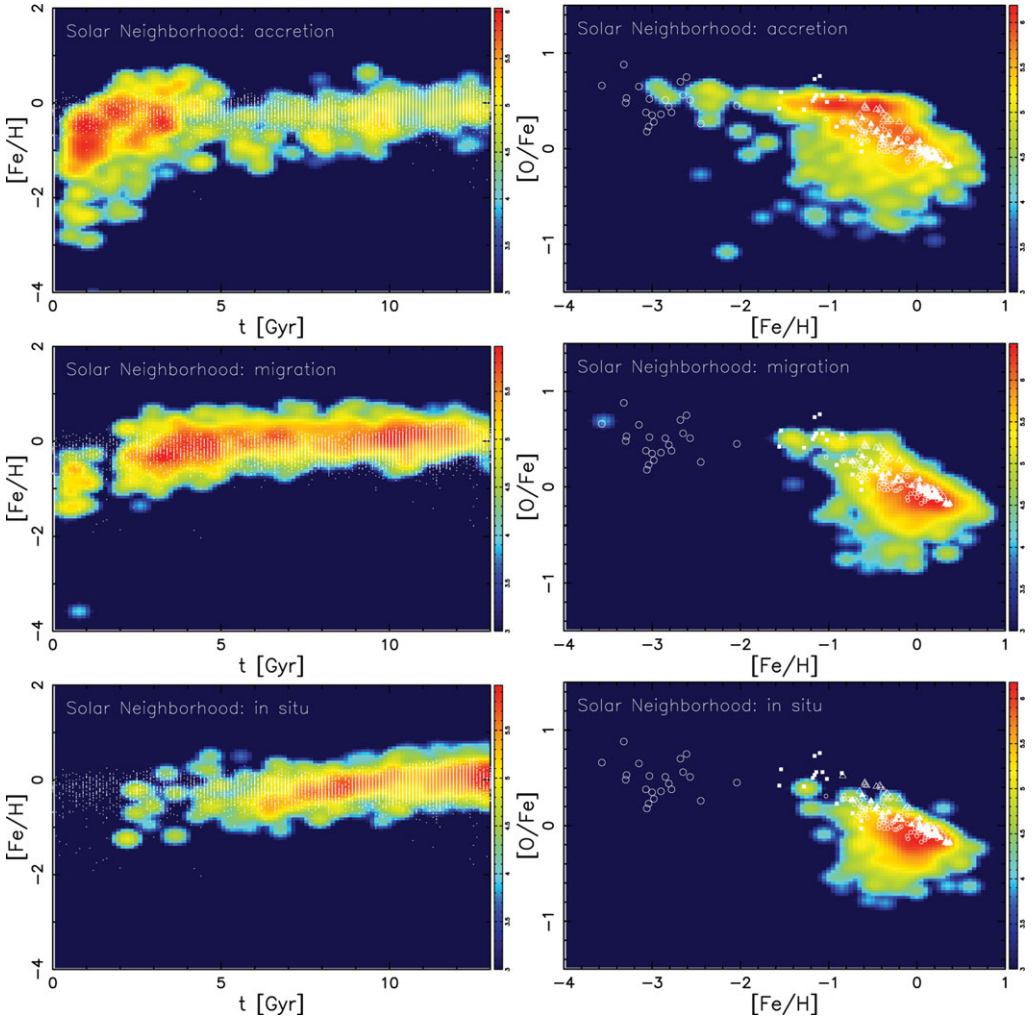

Figure 5. The age-metallicity and [O/Fe]-[Fe/H] relations for stars that formed in-situ (bottom panels), and originated from migration (middle panels) and stellar accretion of mergers (top panels).

https://doi.org/10.1017/S1743921313006339 Published online by Cambridge University Press

abundance patterns of iron-peak elements (low [(Cu,Zn)/Fe] and normal [Mn/Fe]) are also consistent with the yields of low-mass supernovae (Nissen & Schuster 2011, but they made an different interpretation on the abundance patters).

Recently, a number of dwarf galaxies more faint than classical dSphs, called "ultra-faint" dSphs, have been discovered mostly with the SDSS. Fainter dSphs have lower mean metallicities, and at low-metallicities, the elemental abundance ratios may become similar to those of halo stars or they may have a large scatter (see NKT13 for the references).

4. Carbon-Enhanced Damped Lyman α System

Even with the local enrichment from AGB stars, chemodynamical simulations cannot reproduce carbon-enhanced metal-poor (CEMP) stars (Beers & Christlieb 2005). There are various scenarios proposed to explain the carbon enhancement, e.g., faint supernovae, rotating massive stars, binary mass transfer, and interstellar accretion. Recently a similar carbon enhancement has been reported for a very metal-poor damped Lyman α system (DLA) (Cooke *et al.* 2010), which can be explained only with faint supernovae.

Figure 7 shows the elemental abundance ratios from C to Zn relative to Fe, compared with our nucleosynthesis yields of faint supernovae an initial mass of $M = 25M_{\odot}$, metallicity $Z = 0$, and explosion energies: 1×10^{51} erg (SN, solid line) and 20×10^{51} erg (HN, short-dashed line). See Kobayashi *et al.* (2011c) for the details. An efficient mixing-fallback is adopted in both models, black hole masses are as large as $\sim 6M_{\odot}$, and thus the ejected iron mass is much smaller than "normal" SNe/HNe in Kobayashi *et al.* (2006) that are responsible for the chemical enrichment in the Galaxy. Since C is synthesized in the outermost region of the ejecta, [C/Fe] ratio is higher for faint SNe/HNe than "normal" SNe/HNe.

i) The observed large carbon enhancement [C/Fe]$\simeq +1.53$ is well reproduced with our faint SN/HN models. Low-mass AGB stars ($1 - 4M_{\odot}$) can also provide such high [C/Fe]. However, such low-mass stars are unlikely to contribute at the redshift of the C-rich DLA. With the star formation history in the solar neighborhood, [C/Fe] reaches the maximum value at $z = 1.8$ due to the AGB contribution (Kobayashi *et al.* 2011a). ii) The [O/Fe] ratio is higher than for non-faint supernovae ([O/Fe] $\sim 0.5 - 0.6$ for $25M_{\odot}$)

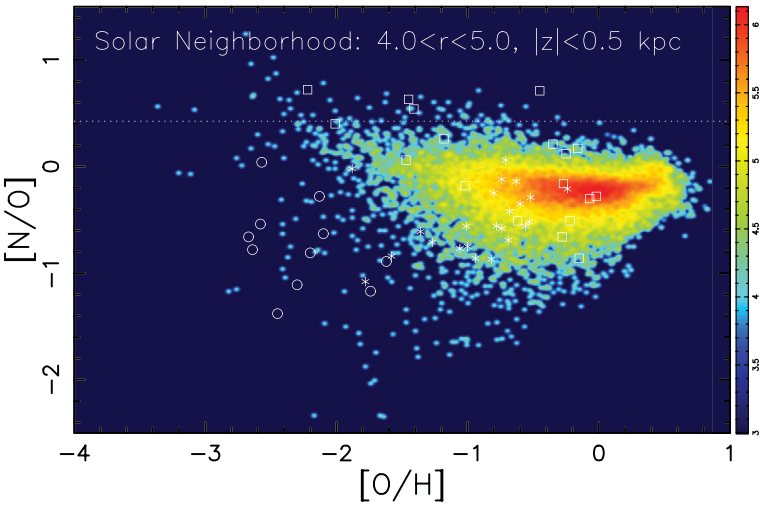

Figure 6. [N/O]-[O/H] relation for the solar neighborhood. See text for the details.

https://doi.org/10.1017/S1743921313006339 Published online by Cambridge University Press

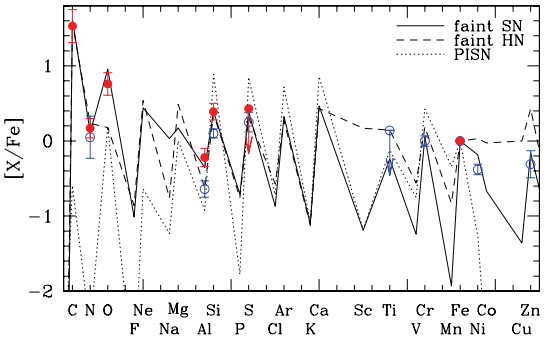

Figure 7. The elemental abundance pattern of the metal-poor C-rich DLA (filled circles) and peculiar DLA (open circles). The solid and short-dashed lines show the nucleosynthesis yields of faint core-collapse supernovae from $25M_\odot$ stars with mixing-fallback. The dotted line is for PISNe from $170M_\odot$ stars.

and is consistent with the faint SN model because of the smaller ejected Fe mass. iii) The [(Si,S)/Fe] ratios are similar to those of non-faint supernovae, and also consistent with the faint SN/HN models. iv) The low Al abundance strongly suggests that the enrichment source is not Pop II supernovae but primordial supernovae. v) The low N abundance is also consistent with the faint SN/HN models, and the high [C/N] ratio cannot be explained with mass loss from rotating massive stars or intermediate-mass AGB stars ($\gtrsim 4M_\odot$).

The dotted line is for the nucleosynthesis yields of the pair instability supernova (PISN) of a $170M_\odot$ star (Umeda & Nomoto 2002). i) The odd-Z effect is much larger than ~ 1 dex. ii) [(Si, S, Ar, Ca)/Fe] are much larger than [(O, Mg)/Fe] because of more extensive explosive oxygen burning. iii) [Cr/Fe] is much larger because of the larger incomplete Si-burning region. iv) [(Co, Zn)/Fe] are much smaller because of the much larger ratio between the complete and incomplete Si-burning regions. All of these characteristics disagree with the observed elemental abundances of these metal-poor DLAs. Even at high-redshift, there is no signature of the existence of PISNe. The [Si/C] for PISNe is as large as +1.5, which is also inconsistent with the observational estimate in the intergalactic medium (IGM, [Si/C] ~ 0.77). The IGM abundance looks more consistent with normal (non-faint) core-collapse supernovae with [C/Fe] ~ 0 and [Si/Fe] ~ 0.7 (Kobayashi *et al.* 2006).

In the early stages of chemical enrichment, the ISM is supposed to be highly inhomogeneous, so that the properties of the first objects can be directly extracted from the comparison between the observed elemental abundances and nucleosynthesis yields. Since the DLA abundances reflect the chemical enrichment in gas-phase, the binary or accretion scenarios do not work. To explain the abundance pattern of the C-rich DLA, enrichment by primordial supernovae is the best solution. Note that not all metal-poor DLAs show C enhancement: Another metal-poor DLA has an abundance pattern that is consistent with normal core-collapse supernovae (Cooke *et al.* 2012). It is important to increase the sample of metal-poor DLAs and to detect heavy elements in metal-poor DLAs as a constraint of the explosion energy. It is interesting that the observed DLA abundance is very similar to those of extremely metal-poor stars in the solar neighborhood including the ultra metal-poor star HE0557-4840 ([Fe/H] $= -4.75$, [C/Fe] $= +1.6$) and BD+44°493. Some of extremely metal-poor stars in dSphs (Norris *et al.* 2010) and the Galactic outer halo (Carollo *et al.* 2012) also show similar carbon enhancement at [Fe/H] $\lesssim -3$. Chemical enrichment by the first stars in the first galaxies is likely to be

https://doi.org/10.1017/S1743921313006339 Published online by Cambridge University Press

driven by core-collapse supernovae from $\sim 20 - 50 M_{\odot}$ stars, which may be consistent with the latest simulations of primordial star formation (e.g., Greif *et al.* 2011).

References

Argast, D., Samland, M., Thielemann, F.-K., & Gerhard, O. E., 2002, A&A, 388, 842
Beers, T. C. & Christlieb, N. 2005, ARA&A, 43, 531
Carollo, D., Beers, T. C., Bovy, J., *et al* 2012, ApJ, 744, 195
Casagrande, L., Schönrich, R., Asplund, M., *et al.* 2011, A&A, 530, 138
Cheng, J. Y., Rockosi, C. M., Morrison, H. L., *et al.* 2012, ApJ, 746, 149
Cooke, R., Pettini, M., Steidel, C. C., *et al.* 2010, MNRAS, 409, 679
Cooke, R., Pettini, M., & Murphy, M. T. 2012, MNRAS, 425, 347
Cresci, G., Mannucci, F., Maiolino, R., *et al.* 2010, Nature, 467, 811
Greif, T. H., Springel, V., White, S. D. M., *et al.* 2011, ApJ, 737, 75
Jones, T., Ellis, R., Jullo, E., & Richard, J. 2010, ApJ, 725, L176
Kobayashi, C., 2004, MNRAS, 347, 740
Kobayashi, C., Karakas, I. A., & Umeda, H. 2011a, MNRAS, 414, 3231
Kobayashi, C., Izutani, N., Karakas, A. I. *et al,* 2011c, ApJ, 739, L57
Kobayashi, C. & Nakasato, N. 2011, ApJ, 729, 16 (KN11)
Kobayashi, C., Springel, V., & White, S. D. M. 2007, MNRAS, 376, 1465
Kobayashi, C., Tominaga, N., & Nomoto, K. 2011b, ApJ, 730, L14
Kobayashi, C., Tsujimoto, T., Nomoto, K., Hachisu, I, & Kato, M. 1998, ApJ, 503, L155
Kobayashi, C., Umeda, H., Nomoto, K., Tominaga, N., & Ohkubo, T. 2006, ApJ, 653, 1145
Maeda, K. & Nomoto, K. 2003, ApJ, 598, 1163
McWilliam, A., Rich, R. M., & Smecker-Hane, T. A. 2003, ApJ, 592, 21
Nissen, P. E. & Schuster, W. J. 2011, A&A, 530, 15
Nomoto, K., Kobayashi, C., & Tominaga, N. 2013, ARA&A, in press (NKT13)
Norris, J. E., Gilmore, G., Wyse, R. F. G., Yong, D., & Frebel, A. 2010, ApJ, 722, 104
Pilkington, K., Few, C. G., Gibson, B. K., *et al.* 2012, A&A, 540, A56
Romano, D., Cescutti, G., & Matteucci, F. 2011, MNRAS, 418, 696
Ruchti, G. R., Fulbright, J. P., Wyse, R. F. G., *et al.* 2011, ApJ, 737, 9
Scannapieco, C., Wadepuhl, M., Parry, O. H., *et al.* 2012, MNRAS, 423, 1726
Schönrich, R. & Binney, J. 2009, MNRAS, 396, 203
Tolstoy, E., Hill, V., & Tosi, M. 2009, ARA&A, 47, 371
Tumlinson, J., 2006, ApJ, 641, 1
Umeda, H. & Nomoto, K. 2002, ApJ, 565, 385
Yuan, T.-T., Kewley, L. J., Swinbank, A. M., *et al.* 2011, ApJ, 732, L14

Discussion

Ivan Minchev: In the age-metallicity relation resulting from your model, you don't see any gradient. Do you think this is a problem?

Chiaki Kobayashi: No. The age-metallicity relation in the solar neighborhood does not show a strong evolution both in my simulation and observations, e.g., Geneva-Copenhagen survey and Casagrande *et al.* 2011.

Schultheis: In the Galactic bulge, we see clearly two distinct populations - metal-rich and metal-poor. Can you reproduce these in your model?

Chiaki Kobayashi: Yes and no. In Figure 4. there is a bimodality in the metallicity distribution function, but these two populations overlap. Two distinct populations are seen in the [α/Fe]-[Fe/H] diagram (Fig. 10 of Kobayashi & Nakasato 2011), metal-rich with low [α/Fe] and metal-poor with high [α/Fe].

https://doi.org/10.1017/S1743921313006339 Published online by Cambridge University Press

Yang Huang: We know that the Milky Way disk has a truncation. Why I don't see such a feature in your plot of metallicity radial gradient?

Chiaki Kobayashi: There is no truncation seen in metallicity gradient up to 20 kpc in my simulation. If there is a truncation of metallicity in the Milky Way disk, the star formation recipe may have to be revised.

Juntai Shen: Bar is not very prominent in your simulation. Can you reproduce the boxy shape and cylindrical rotation of the Galactic bulge?

Chiaki Kobayashi: Not yet. A bar-like structure can be seen in my simulation, but higher resolution is needed for further analysis.

Hans-Günther Ludwig: I would like to get a feeling for the theoretical uncertainties of your modelling results: How many realizations (initial condition and parametrization of small-scale physics) go into your final abundance results which you compared to observations.

Chiaki Kobayashi: I've used ~ 100 initial conditions with low resolutions, ~ 5 had a good disk, and chose this one. For the best initial condition, with higher resolution, I've tested ~ 10 parameter sets. Important parameters are the star formation timescale and feedback radius, which are constrained from the metallicity distribution function. See Kobayashi & Nakasato 2011 for the details.

Hans-Walter Rix: You showed plots that separated the impact of different effects (in situ, accretion, migration) on the age-abundance patterns. Can you say how you separated those there effects in your simulations?

Chiaki Kobayashi: Accretion means stellar accretion of satellite galaxies. The separation is made by looking back the locations when the stars formed in the simulation.

Birgitta Nordström: You said that the origin of the thick disk is 50% minor mergers. Do you think it is possible to formulate criteria for which stars come from which effect?

Chiaki Kobayashi: The origin can be separated only when I trace back the orbit of particles in simulations, and the fraction slightly depends on the details of the analysis - the definition of membership of satellite galaxies for example. It is difficult to determine the origin from the available observations of stars. The stars with a different origin can have similar kinematics or α enhancement.

Eline Tolstoy: How do you include observational errors in your simulations when you compare with observations. This is extremely important for accurate comparison between models and data. You should 'observe' your models.

Chiaki Kobayashi: I just take into account observational errors when I draw a conclusion from the comparison. I'll let somebody else to do more accurate comparison. Because of the resolution, the star particle in simulations is not a single star. So we have to generate stars from star particles, apply additional effects such as dust extinction and binarity, then take account of observational selection bias and errors...

https://doi.org/10.1017/S1743921313006339 Published online by Cambridge University Press